This is the accepted version of the article published in *IEEE Sensors Journal*.
DOI: 10.1109/JSEN.2025.3607761

IEEE Sensors Council

Soft Transducers with Notch Filters for Spatially-Distributed Strain Sensing

Anthony Wertz, *Member, IEEE*, Dylan Shah, , and Carmel Majidi, *Member, IEEE*

***Abstract*— Sensor arrays for soft and stretchable electronics typically require a large number of electrical leads that scale with the number of sensing nodes within an array. Whereas rigid electronics can incorporate transistors and complex CMOS architectures for sensor multiplexing, soft material circuits are largely limited in how individual sensing nodes can be addressed. To overcome this challenge, we introduce an approach that utilizes a variable-frequency notch filter to encapsulate resistive or capacitive soft-material and rigid sensors for use in the detection of phenomena including material strain, applied force, and temperature. This design builds on the rich and growing body of research using capacitive and resistive soft material sensors, providing a customizable framework on which to build distributed sensing networks. In particular, we investigate how incorporating strain-sensitive components into a notch filter enables tuning of the sensor's sensitivity, independent of the particular capacitor or resistor design, allowing sensor responses to be isolated and allow network reconfiguration without calibration. Our approach offers a straightforward means of connecting multiple sensors, even of different types, in a common sensing network with minimal wiring and interface requirements. The active filters were designed to fit in a small area and require minimal rigid components to facilitate incorporation into highly stretchable or bendable soft systems.**

***Index Terms*— notch filter, soft sensors, soft robotics**

I. Introduction

DISTRIBUTED, multi-modal sensor networks are important in soft robotic applications, including closed-loop manipulator control, state estimation, and large-area tactile sensing [1], [2]. Truby, Della Santina, and Rus show it can be quite difficult to infer the state on a continuum manipulator without sufficient sensorization [3]. Even after a kinematic model has been derived, machine learning or other calibration is often still needed to achieve accurate proprioception. Shah, Woodman, Buckner, *et al.* further demonstrate the utility of sensor integration in soft robotics applications [4]. As described by Hegde, Su, Tan, *et al.*, soft or deformable robots have many more possible state configurations compared to traditional rigid devices, so dense sensorization is often necessary [5]. Similarly, distributed sensing is useful in wearable and electronic skin applications [6]. In part, distributed networks can be used for denser sensing over a wide area or complicated geometry, needed in virtual reality and haptics [7] and tactile sensing [8]. It can enable estimation of the shape of an irregularly shaped or transforming object, important in biomedical and agricultural applications. Shah, Woodman, Sanchez-Botero, *et al.* implemented shape-sensing sheets by combining inertial measurement units and capacitive sensors at nodes along a planar substrate [9]. However, they noted that it can be difficult to scale such systems due to challenges addressing and interfacing numerous discrete sensors. Because soft sensors and electronics lack the complex multiplexing capabilities of rigid circuits and CMOS-based architectures, the number of electrical leads required for addressing typically scales with the number of sensing nodes.

Our work addresses this key challenge in soft sensor arrays through the use of a variable-frequency notch filter that allows each sensing node to share the same set of electrical leads for addressing and interfacing. In operation, our approach is similar to strain detection in fiber Bragg gratings that form notch filters by reflecting particular light wavelengths [10]. However, the silica and plastic optical fibers used in these scenarios typically have low yield strains (a few percent) and limited reconfigurability. Other researchers tried to address tunability by designing multi-material systems [11], but this is considerably more complicated than our proposed method of replacing a few passive components in the filter design. To enable distributed (multisegment) strain sensing using minimal wires, we propose a filtering framework that addresses three main challenges inherent in previous research:

Anthony Wertz was with the Robotics Institute, Carnegie Mellon University, Pittsburgh, PA 15213 USA (email: awertz@cs.cmu.edu), now with Latitude AI, Pittsburgh, PA 15222.

Dylan Shah is with Arieca, Pittsburgh, PA 15208 (email: dshah@arieca.com

Carmel Majidi is with the Department of Mechanical Engineering, Carnegie Mellon University, Pittsburgh, PA, 15213 USA (email: cmajidi@andrew.cmu.edu)

1) **Active-filtering and buffering**: Each sensor node incorporates a high input-impedance active filter with a buffered output, decoupling each node from all others in the network. This approach eases reconfiguration and supports heterogeneous sensor networks as well.
2) **Tunable notch filter topology**: Resistive and capacitive sensing elements are embedded in notch filters whose center frequencies and sensitivities can be adjusted independently of the native properties of the sensor.
3) **Operational frequency in accessible ranges**: By selecting appropriate component values, we achieve sensing performance at more moderate operational frequencies than previously demonstrated with the passive LC filter designs, allowing for better spectral usage and operation in frequency ranges more accessible to compute-limited devices.

We describe our framework design using a soft capacitive strain sensor encapsulated in a notch filter, derive gauge factors and theoretical supported sensor densities, and demonstrate precise strain tracking and sensor decoupling. This is done both in simulation and physical hardware using liquid-metal based capacitive sensors. We use this embodiment as a case study to investigate the behavior of the proposed filter and sensing mechanism, agnostic of the particular physical hardware it is run on. The integrated soft system design described in this work offers many advantages both for on-body sensing in areas that undergo much larger strains, such as joints, or when wearability is a large factor. This robust design and ease of use may serve as a useful model for future distributed sensor designs that require minimal interface requirements, easy tuning, dense networks, and reliable interfacing.

A. Background

There is a significant amount of existing literature on capacitive and resistive sensors that are soft and stretchable [8]. A prevalent strategy for designing such devices is the use of liquid-metal embedded elastomers (LMEE), as described by Majidi, Alizadeh, Ohm, *et al.* in [12], as it proves to be a versatile tool for the implementation of stretchable circuits and integration of soft devices with rigid counterparts. For example, highly stretchable strain gauges can be designed using LMEE. Nesser and Lubineau review many examples of capacitive strain gauges [13], and Wu, Peng, Yu, *et al.* discuss resistive and capacitive sensors and strategies to incorporate them into designs [14]. Souri, Banerjee, Jusufi, *et al.* go into even greater detail on the incorporation of such devices in wearable applications [15].

Distributing sensing is a different objective with its own set of challenges. Incorporating traditional rigid sensing chips distributed across many sensor cells can be challenging both to wire appropriately and to scale, as many devices and communication protocols have limited device addresses available, requiring multiple communication buses or complicated multiplexing [9], [16]. In some works [4], [17], sensors are handled directly without an interfacing chip. This requires a new data wire for each sensor, drastically limiting how many sensors could be physically connected in a particular application and increasing the stretchable wire count, a notable failure point in stretchable electronics. Sensors are sometimes distributed in matrices to reduce the data lines required for interrogation from n to $\sqrt{n}$ [18]. However, this is the best case reduction, assuming that the devices are connected in a matrix fashion. Doing so may greatly limit the distribution geometries achievable and might not be relevant at all for oddly-shaped structures as occur frequently in biology. In addition, $\sqrt{n}$ may still be quite large for a small wearable system to interface with.

In other instances, clever mechanical design and signal processing techniques might be used to decouple localized signal contributions and infer a distributed response over a single sensor. White, Yuen, and Kramer measured localized deformation on a monolithic capacitive sensor taking advantage of the reduced electrical transmission with distance when capacitor electrodes were made to have fairly high resistance [19], with a more mathematically rigorous description of this effect by Tairych and Anderson in [20], [21]. Tairych and Anderson derived the analytic expression for three capacitive strain sensors in series, but even with so few sensors, there was considerable cross-talk and scaling up that approach would be quite cumbersome [20]. Similarly, Sonar, Yuen, Kramer-Bottiglio, *et al.* performed touch localization on a two-dimensional substrate using the same concept [22]. The array can then be interrogated by varying the input frequency and training a machine learning model to classify the individual "pixel" locations. This approach does not easily lend itself to complicated geometries, larger sensing areas, or reconfigurability, and requires data collection and retraining for any new device or geometry. Bai, Li, Barreiros, *et al.* used light-absorbing dyes embedded in a stretchable fiber core to distribute sensing along the device that change the color of the received light depending on where deformation occurred and what kind [23]. The design was greatly limited in the geometry supported. Hellebrekers, Kroemer, and Majidi performed contact localization by modeling changes in the magnetic field with the deformation of a magnetized polymer [24]. A black-box machine learning model was trained on experimental data to associate a modified magnetic field with a mechanical indentation in a particular region of the polymer. There was a limit to the number of sensors that can be connected in a single system, and quite a bit of data was required for collection as described by Bhirangi, Hellebrekers, Majidi, *et al.* [16].

Artificial intelligence methods are commonly used to model soft system sensor behaviors, including hysteresis and fatigue, including work by Kim and Park [25] building on top of more traditional models, such as the Preisach model [26]. As they detailed, the small signals coming directly from typical soft strain sensors are noisy and not always easy to process. Funabashi, Isobe, Hongyi, *et al.* use graph convolutional networks to utilize tactile information distributed over an Allegro hand [27]. However, such methods typically fail to isolate particular sensors in a single network when their signals mutually interfere and their response depends on the particular network of sensors in a given configuration. Instead, it is desirable to keep the sensor feedback isolated between devices.

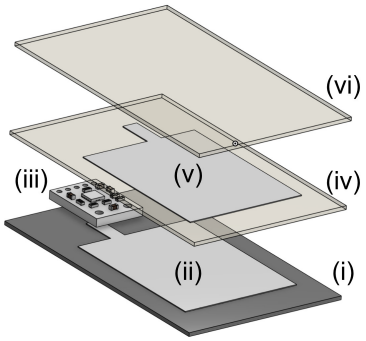

(a) Device material stackup.

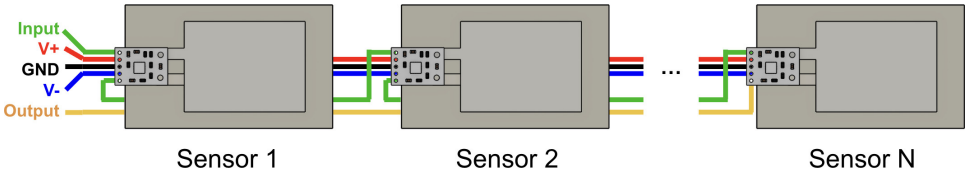

(b) Multi-sensor connection schematic.

(c) Fabricated sensor at zero strain.

(d) Fabricated sensor at $\sim$200 % strain.

Fig. 1: (a) The sensor device stackup. [i] VHB substrate with [ii] patterned OGaIn capacitor electrode and [iii] notch PCB, covered with [iv] dielectric VHB, patterned with the [v] second OGaIn electrode, sealed with more [vi] VHB. (b) Multi-sensor serial connection schematic with a five-wire network interface. (c) A fabricated sensor, relaxed with zero strain. (d) The same sensor with $\sim$200 % strain.

In 2022 Kim, Kim, and Park demonstrated a distributed soft sensor network with a single input and a single output that used passive inline LC bandpass filters to selectively interrogate different sensors by varying the frequency of an input sinusoid and analyzing the attenuation of the signal at the output [28]. Strain-sensitive resistive elements were used to modulate the attenuation based on the applied force. However, to maintain sensor bandwidths to reasonably low frequencies, high component values are needed for the inductor and capacitor selection. This is at odds with the increasing impedance of inductors at higher excitation frequencies and higher inductances. Sensor bandwidths in [28] ranged from about 280 kHz to 3 MHz, which requires high-rate data acquisition and computationally expensive processing of raw sensor data. Similarly, Kim, Kim, and Park also demonstrated a modular sensor network for distributed force and human touch detection [29]. The same passive LC bandpass filters were utilized in parallel, each with a force-sensitive series resistance, forming a network of notch filters in which the depth of the notch was modulated by the force contact and the frequency shifted by capacitive effects of a finger in contact. The network suffered from similar issues as the bandpass implementation, namely the operating range varied from 500 kHz to 5 MHz this time. Furthermore, the use of a passive network made decoupling complicated, requiring a compensation algorithm to reduce the effects of new sensors, an approach likely to be brittle in the face of system reconfigurations or component degradation. In both cases, the LC networks offer much more limited options for frequency tuning, as component values for inductors and capacitors in usable ranges are fairly limited and have high tolerances.

Existing approaches illuminate the central challenges in distributed sensing for soft robots and wearable devices. Integrated sensor chips often have finite addressing capabilities, forcing the use of multiplexing, complex PCB layouts, multiple communication buses, or one-wire-per-sensor solutions. Systems that rely on large amounts of training data for calibration or fixed hardware addresses for individual sensors can be difficult to scale to larger networks or adapt to new geometries and sensor types. Passive LC filter networks can reduce wiring, but suffer from crosstalk and require careful component selection to achieve reasonable performance. Encapsulation in a simple active filter can overcome these challenges without adding excessive computational, space, wiring, or power requirements that come with more complicated multiplexing strategies.

II. Theory of Operation

The overall design of the soft sensing array is presented in Fig. 1. A stretchable, strain-sensitive capacitor was formed by patterning metallic paste electrodes onto stretchable foam VHB tape and connecting this capacitive sensor to a notch filter (Fig. 1a). The device fabrication is described more completely in section III-A. Sensors can then be connected sequentially on the same bus, sharing all of their interconnects.

Fig. 1b shows a schematic of the sensor network we fabricated, including node-to-node connectivity. Crosstalk did not contribute noticeably to the signal, but just as in rigid devices, suboptimal conductor layouts and higher frequencies could lower the signal-to-noise ratio. The fabricated sensors were stretched up to ∼200% strain during operation (Fig. 1c- 1d). In this section, we detail the design and theory of operation of the proposed sensing arrays.

A notch filter is another name for a bandstop (also bandreject) filter with high attenuation over a very narrow bandwidth, ideally a single frequency. An infinitesimally small bandwidth is not realizable in practice, but the degree to which this constraint is satisfied in a practical circuit can be quantified using the *quality factor*, or Q-factor. This and other common filtering concepts can be understood more thoroughly with any number of analog filtering textbooks, such as that by Williams [30]. The Q-factor can be interpreted as the filter frequency over the half-power bandwidth, i.e., $Q = f_0/\mathrm{BW}_{3\,\mathrm{dB}}$. A narrower bandwidth is indicated by a higher Q-factor.

Typically, the notch frequency is static, for example in the case of 60 Hz mains hum rejection. As the notch frequency is usually controlled by a few particular resistor and capacitor values, replacing them with variable-resistance or -capacitance devices yields a variable notch frequency, which can be interpreted as a sensor output. Spectral separation of multiple notch filters through appropriate selection of components allows for sensor response isolation and identification in a distributed network. The entire sensor network can be interrogated using a single variable-frequency "chirp" that covers the spectral bandwidth of interest. We show that this encapsulation offers some considerable advantages over typical bare-sensor designs. The framework is agnostic to the particular notch implementation, although there are trade-offs using one over the other. This work focuses on the Bainter notch topology, but the twin-T notch was also considered for comparison in the supplemental material. The Bainter notch was a better choice for our particular implementation because of the very low capacitance of the fabricated strain sensors. For further discussion of the twin-T results, refer to the SI.

The general form for a second-order notch transfer function is

$$H(s) = \frac{s^2 + \left(\frac{\omega_z}{Q_z}\right) s + \omega_z^2}{s^2 + \left(\frac{\omega_p}{Q_p}\right) s + \omega_p^2} \tag{1}$$

where ω_z and Q_z are the radial frequency and quality factor of the zeros (respectively), and ω_p and Q_p are those of the poles. A symmetric notch has unity gain before and after the notch frequency and is formed when both the pole and zero frequencies are equal, $\omega_z = \omega_p = \omega$. To achieve a narrow bandwidth, high quality factors are desired for both the pole and zero. However, Q_z must be greater than Q_p by at least an order of magnitude. In the case where they are equal, the numerator and denominator effectively decrease at the same rate, yielding a unity response and producing no notch at all. When Q_p is larger than Q_z, the denominator decreases faster, leading to a *gain* instead of attenuation. Ideally, Q_z is reasonably large (e.g., $Q_z \geq 10^3$), allowing for a deep notch, and Q_p is at least 10, providing a narrow bandwidth. At most, Q_p is one order of magnitude lower than Q_z, otherwise the depth of the notch will begin to reduce. A shallow notch is not terribly consequential so long as the frequency can be estimated accurately, but a narrower bandwidth is desirable to avoid occlusions if many devices will operate in close spectral proximity.

A. Bainter notch

A Bainter notch [31] (Fig. 2), can be designed to yield a high-pass, low-pass, or symmetric notch response with tunable frequency and Q-factor. While other notch topologies have quality factors Q_z that are mainly dependent on the filter's RC components, the Bainter notch does not. The quality factor in the numerator is

$$Q_z = \sqrt{\frac{R_1 C_1 A(A+1)}{4 R_2 C_2}} \approx \sqrt{\frac{R_1 C_1 A^2}{4 R_2 C_2}} = A\sqrt{\frac{R_1 C_1}{4 R_2 C_2}}. \tag{2}$$

where A is the operational amplifier gain. Given the proportionality with the amplifier gain, so long as a high-gain amplifier is selected (e.g., $A \geq 10^4$) we can design a large Q_z, at which point the first-order term can be ignored in the analysis. Because the sensor network does not drive a large load, the power requirements are minimal and high-frequency, small-form factor devices are readily available and easily integrated. We can calculate Q_p as

$$Q_p = \sqrt{\frac{R_2 C_2}{R_1 C_1}} \tag{3}$$

and the notch frequency lies at

$$f_{\mathrm{notch}} = \frac{1}{2\pi}\sqrt{\frac{1}{R_1 R_2 C_1 C_2}}. \tag{4}$$

To make a variable-frequency notch, some of the resistors or capacitors that define the notch frequency need to be replaced with variable-resistance or variable-capacitance sensors. Consider a soft strain gauge as a concrete example. The schematic in Fig. 2 highlights capacitor C_1 to be replaced with a strain-responsive element, along with components R_2 and C_2 that will be used to tune the notch frequency and Q_p. Alternatively, the resistor could have been selected as the strain-responsive element. Resistive and capacitive strain gauges have advantages and disadvantages. Wu, Peng, Yu, *et al.* provide an excellent review of resistive and capacitive sensing approaches and their relative strengths and weaknesses in [14], and Nesser and Lubineau give a more detailed evaluation of capacitive strain sensing in particular [13].

Passive elements do not need to be completely replaced with strain-responsive variants. Instead, they can be added in series with or in parallel to fixed elements to tune the sensitivity. We consider *direct* replacement of the passive element with a strain-responsive variant, an *additive* fixed element, or a *reciprocal* fixed element. The *additive* and *reciprocal* qualifiers

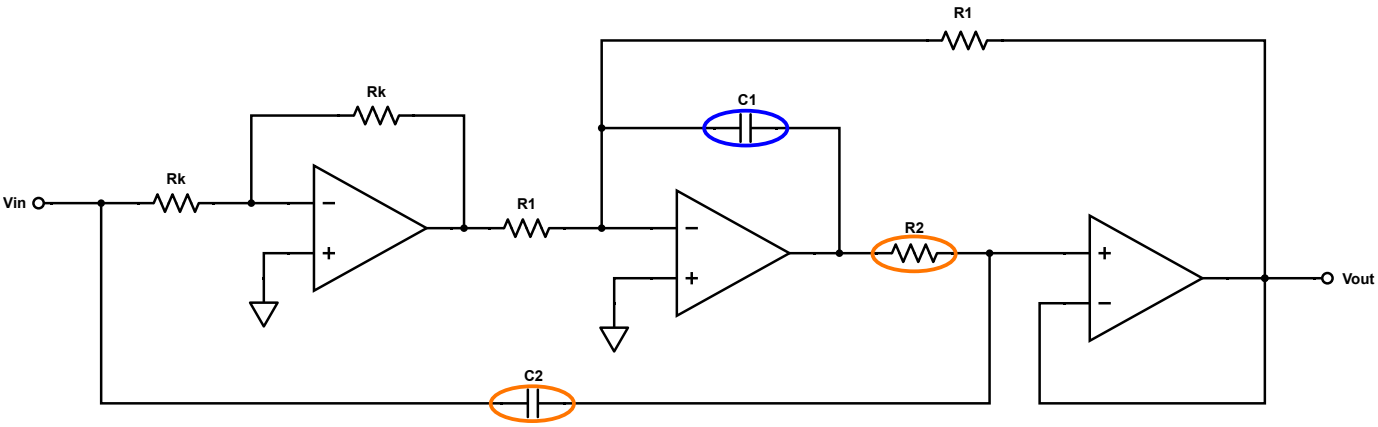

Fig. 2: Bainter notch filter topology. The components chosen to be strain-responsive are circled in blue, and fixed elements used to design the notch frequency are circled in orange.

assist in analyzing the behavior of the circuit under functionally equivalent modifications to different passive elements. Adding a resistor R_{new} in series to R_{old} is an *additive* modification, as $R = R_{old} + R_{new}$. If added in parallel, the effect is *reciprocal* in nature, $1/R = 1/R_{old} + 1/R_{new}$. If a fixed capacitor is added, the topologies are reversed: adding capacitors in parallel yields an *additive* effect on total capacitance, while adding them in series yields a *reciprocal* change. We report gauge factors for the Bainter notch next, but note that the SI contains much greater treatment of the subject for both Bainter and Twin-T notches, and more thoroughly explores the differences in signal response.

B. Effective gauge factor

Suppose that a capacitor is directly replaced with a capacitive strain gauge with a gauge factor G_c, defined as

$$G_c = \frac{\Delta C/C_0}{\varepsilon}. \tag{5}$$

with strain $\varepsilon = \Delta\ell/\ell_0$ (the fractional change in unstrained length ℓ_0), and C_0 is the capacitance at zero strain. An ideal parallel-plate capacitor has a unity gauge factor. Rearranging (5), noting that $\Delta C = C + C_0$, the capacitance at a particular strain is $C = C_0(1 + G_c\varepsilon)$. We can calculate the effective gauge factor, that is, the frequency response to strain, as

$$\frac{f - f_0}{f_0} = \frac{1 - \sqrt{G_c\varepsilon + 1}}{\sqrt{G_c\varepsilon + 1}} \tag{6}$$

where f_0 is the unstrained notch frequency. The effective gauge factor for a direct replacement is

$$G_{f,\text{direct}} = \frac{\Delta f/f_0}{\varepsilon} = \frac{1}{\varepsilon}\left(\frac{1 - \sqrt{G_c\varepsilon + 1}}{\sqrt{G_c\varepsilon + 1}}\right). \tag{7}$$

The effective gauge factor is dependent only on the capacitor's gauge factor and the strain itself. Substituting a strain-sensitive resistor instead yields the same effective gauge factor. Assuming the gauge cannot be compressed smaller than ℓ_0, using an element with a positive gauge factor implies a negative frequency response to strain. This is the case for a parallel plate capacitor which has a gauge factor around $G_c = 1$. Using a comb capacitor instead with a gauge factor of around $G_c = -2$ would lead to an increase in frequency in response to strain. It also introduces a pole in the gauge factor at $\varepsilon = -1/G_c$ as the capacitance drops to zero and causes the notch frequency to approach infinity. The choice of a negative or positive gauge factor adds some design flexibility, depending on whether it is desirable to have the response grow more slowly (positive) or more quickly (negative) with increasing strain.

Adding a fixed capacitor in parallel, an *additive* configuration, yields a total capacitance of $C = C_{fixed} + C_0(1 + G_c\varepsilon)$. To normalize the analysis, let the constant $k = C_{fixed}/C_0$ relate the capacitance of the fixed component to the unstrained capacitance of the sensor. With this we have $C = C_0(k + 1 + G_c\varepsilon)$. The gauge factor is then

$$G_{f,\text{additive}} = \frac{1}{\varepsilon}\left(\frac{\sqrt{k+1} - \sqrt{G_c\varepsilon + k + 1}}{\sqrt{G_c\varepsilon + k + 1}}\right). \tag{8}$$

In this way, a fixed component can be added to modify the sensitivity of the response. These results are identical for resistive strain gauges when adding fixed resistance in series, also an *additive* configuration.

Adding a fixed capacitor in series, a *reciprocal* configuration, yields a total capacitance of $1/C = 1/C_{fixed} + 1/(C_0(1 + G_c\varepsilon))$. Substituting in k, the resulting gauge factor is

$$G_{f,\text{reciprocal}} = \frac{1}{\varepsilon}\left(\frac{\sqrt{G_c\varepsilon + k + 1} - \sqrt{k+1}\sqrt{G_c\varepsilon + 1}}{\sqrt{k+1}\sqrt{G_c\varepsilon + 1}}\right). \tag{9}$$

When the gauge factors are positive, the direct configuration sets an upper bound on the responsiveness of the sensor, starting at a value equal to the gauge factor of the underlying resistive or capacitive strain sensor and then decaying to zero with increased strain. The initial value and the decay rate can be tuned by using an additive or reciprocal configuration and modifying k.

When the gauge factors are negative, as in the case of the comb capacitor, the behavior looks quite different. Once again,

the direct configuration gives an upper bound on the response rate. In this case, the frequency shift increases slowly with strain to start, but increases rapidly near the singularity. The parameter k can be used once more to tune the curve, this time moving the asymptote somewhere convenient. Unlike in the previous case, the effective gauge factor can be substantially higher than that of the strain sensing element.

Not included above are the cases where both the resistive and capacitive elements are made to be strain-responsive. These results can be found in the supplementary material.

III. Implementation and Validation

A. Device fabrication

Printed circuit boards (PCBs) were designed with a notch circuit and terminals to connect strain-sensitive capacitors. Double-sided VHB tape (3M) was used as both the device substrate and the dielectric for the strain-sensitive capacitors. As with previous methods to create soft capacitive sensors, VHB tape was selected because it is soft, elastic, and adhesive on both sides [32], [33]. Elastic parallel-plate capacitors were fabricated by patterning electrodes with oxidized eutectic gallium-indium liquid metal paste (OGaIn) on either side of the VHB using stencils cut with a CO_2 laser. The PCB was pressed in place on the patterned VHB. A conductive, biphasic liquid metal ink [34] was used to securely connect the OGaIn electrodes to the PCB pads. To prepare the ink, styrene-isoprene-styrene block co-polymer (432393, styrene $14\,\%$ by weight, Sigma-Aldrich) was dissolved in toluene in a ratio of 25:75 by weight. The dissolved SIS was combined in a vial with silver flakes (41-071, Technic) and eutectic gallium-indium (EGaIn) in a weight ratio of 1:2:5. The vial was mixed using a planetary mixer (AR-100, Thinky) at $2000\,\mathrm{rpm}$ for three minutes without defoaming. The contents were mixed by hand with a tongue depressor for about one minute and then mixed in the planetary mixer for another three minutes. The ink was poured into a syringe and dispensed by hand. Finally, clear tape (Scotch tape, 3M Inc.) was added as a stiffener on both ends to form reliable clamping points for characterizing the device's strain response. Assembled notch sensors could be strained to $\sim 200\,\%$ (Fig. 1c and 1d).

B. Experimental setup

1) Hardware configuration: The strain response of the fabricated sensors was evaluated using a universal testing system (5969, Instron) to perform controlled tensile tests. Both ends of the device were clamped in place, with one end free to stretch the sample. With a filter in place, the notch frequency was determined by chirping the input and looking for notches in the estimated transfer function. Chirps were generated using a direct digital synthesis (DDS) IC (AD9833, Analog Devices) controlled by a hobbyist microntroller (Feather nRF52840 Express, Adafruit) to scan for notches from $1\,\mathrm{kHz}$ to $100\,\mathrm{kHz}$. A logarithmic chirp was used, as it spreads the spectral energy uniformly over each decade. The chirp frequency at a particular time is calculated as $f(t) = f_0(f_1/f_0)^{t/t_1}$, where f_0 and f_1 are the starting and ending frequencies of the chirp, respectively, and t_1 is the length of the chirp in units of t. This assumes that the chirp starts at time $t = 0$. Chirp boundaries were marked with GPIO transitions and captured using a logic analyzer (Logic 8, Saleae). The logic analyzer was also used to record the chirp input and the sensor output at $1.25\,\mathrm{Mbps}$, more than ten times the search bandwidth for better signal reconstruction and to reduce aliasing artifacts. The low-voltage DDS output was buffered and amplified from $0.65\,\mathrm{V_{pp}}$ to $4.5\,\mathrm{V_{pp}}$ to better cover the ADC range. Data were captured continuously throughout the extension and relaxation of the sensor.

The unstrained capacitances of the sensors were measured and fixed components were chosen with reasonably tight tolerances for the filters, less than $1\,\%$ for resistors and $5\,\%$ for capacitors. The assembled filters were cyclically strained and relaxed using an Instron to record precise measurements of the tensile strain.

2) Notch frequency detection: Both the input chirp and filtered output were sampled to estimate the frequency response to ensure robust notch detection in the face of noise and interference. For each chirp, the transfer function was estimated as $\widehat{H}(f) = S_{xy}(f)/S_{xx}(f)$, where S_{xx} is the power spectral density (PSD) of the input and S_{xy} is the cross power spectral density (CPSD) of the input and output. Both were estimated using Welch's method [35] which averages periodograms computed on overlapping time segments to reduce noise. The estimated transfer function was smoothed using a Savitsky-Golay filter [36], an efficient least-squares fit of a low-order polynomial over a short window to smooth the data without removing important features. The notch frequency was then identified by searching for a minima in the transfer function over the sensor's bandwidth.

3) Strain estimation: Using the measured notch frequency shift, the strain could be directly estimated using the effective gauge factor derived previously. We only need to assume or measure the capacitive gauge factor. For the parallel plate capacitors implemented, the gauge factor should be close to unity, i.e., $G_c = 1$. Sensor data were also directly fit to the appropriate model to better account for any nonideal components and parasitic capacitances. A constrained least-squares fit using the Levenberg-Marquardt algorithm [37] was used to identify the unstrained notch frequency and sensor gauge factor.

C. Sensor validation

1) Single-unit strain tracking: The measured frequency shift of the notch is superimposed over the strain in Fig. 3, top. The sensor was cyclically strained to $100\,\%$ five times. A bowed effect is observed due to the non-linearity of the sensor response, exhibiting a larger frequency shift for lower strains and a lower response at higher strains. The shift was fit to the direct attachment sensor model described previously. Doing so yields a near perfect fit to the data, as shown in Fig. 3, bottom, with a strain estimation error less than $0.5\,\%$. The fit gauge factor was $G = 0.95 \pm 0.05$ standard error, close to the expected $G = 1$ for a parallel-plate capacitor. The fitted zero-strain frequency was $f_0 = 26\,\mathrm{kHz} \pm 1.5\,\mathrm{kHz}$ standard error, very close to the expected frequency based on the model, about

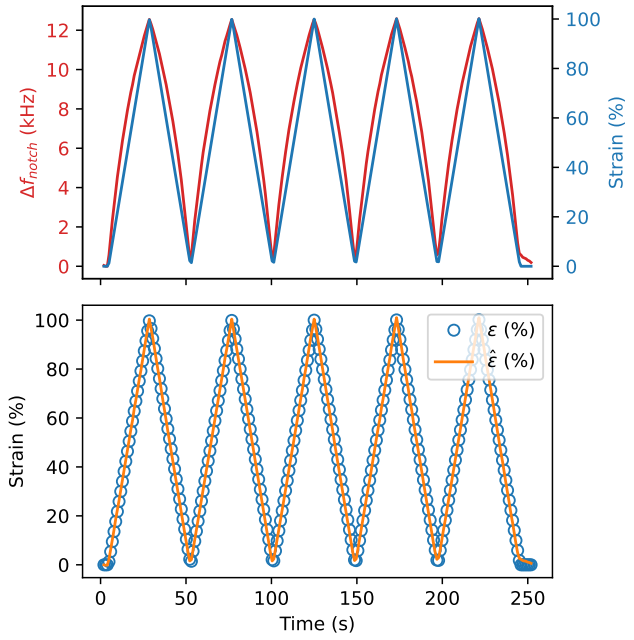

Fig. 3: (Top) Measured device strain (blue) and sensor frequency shift (red). (Bottom) Estimated versus measured strain after fitting. ε (blue circles) is the measured strain and $\hat{\varepsilon}$ (orange line) is the estimated strain based on the sensor frequency shift.

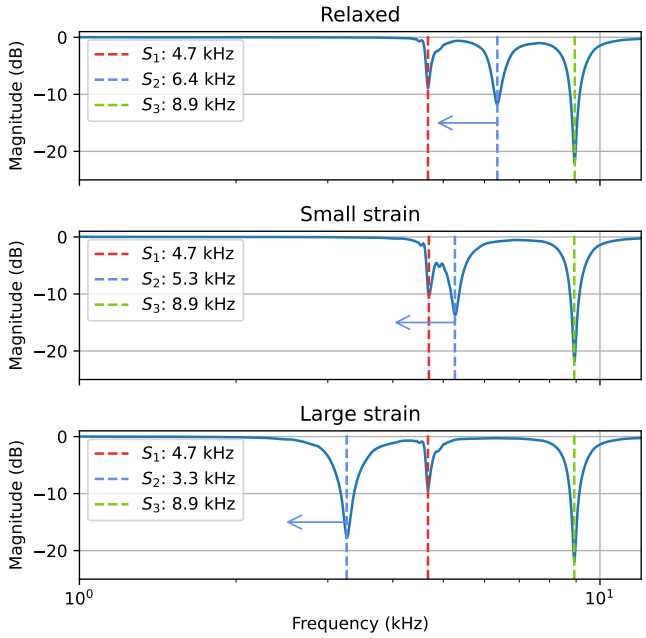

Fig. 4: Multi-sensor notch detection on a three-sensor homogeneous sensor network using Bainter notches, labeled S_1, S_2, and S_3 in the figures. The top plot shows the zero-strain response. The center sensor S_2 was then strained to shift the notch frequency down, eventually overlapping (middle) and passing through (bottom) the first sensor notch.

24.8 kHz. The difference may be due to parasitic capacitances, although the measured values were within 5 %.

2) Multiple-unit strain tracking: A notable strength of notch filter encapsulation is that it enables the removal or incorporation of sensors on a network without requiring recalibration or compensation. To incorporate multiple sensors in a single network, multiple notches must be identified and associated with the correct sensor. Ideally, each sensor would exhibit a frequency response strictly within the desired frequency band, making sensor disambiguation trivial. In section IV we suggest design guidelines using this strategy. At a high level, the exact same approach was followed for the single-sensor detection, except that the peak detection was done independently for each sensor's bandwidth.

To demonstrate the approach experimentally, we fabricated three notch sensors with different zero-strain notch frequencies and placed them on the same network. Using a single chip, we observed distinct peaks and could easily detect each notch (Fig. 4). The three panels demonstrate complete decoupling of the signals, even as one sensor is strained so that its notch frequency overlaps with and eventually passes through another sensor's notch.

Due to sensor cell decoupling, networks can be easily reconfigured without requiring a network calibration step or complicated compensation algorithms required in other works. Heterogeneous sensing networks can also be formed: so long as the sensors used transduce the signal of interest to a change in resistance or capacitance, they can be encapsulated in a notch filter and incorporated into the network. This includes strain sensors, thermistor temperature sensors, and pressure sensors. Aside from ensuring devices on the same network do not use conflicting frequency bandwidths, there is no additional work to be done to reconfigure sensors on a different network. Adding sensors does not substantially impact the computational load on the system, as their responses are detected on a single chirp. If the sensor bandwidths are mutually exclusive, there is almost no difference. Sensor sampling frequency is only dependent on the designed notch frequencies and the ADC sampling rate, not the sensor count, although at high sampling frequencies the chirp period becomes much smaller, so it can be more difficult to distribute the chirp energy uniformly across the frequency spectrum to generate a usable signal-to-noise ratio. At higher sampling rates, the spectrum has more noise, but it still exhibits well-defined notches. We evaluated sampling rates from 1 Hz to 100 Hz further in the SI.

IV. Network Design and Theoretical Limits

There are a number of ways to implement a distributed sensor network using this framework, depending on the design objectives. Here, two procedures are highlighted to illustrate the capabilities and limitations of this network design and to lay the groundwork for incorporation into new applications. We additionally derive examples of other networks, to provide insight into the the generality of the proposed sensing framework. The first approach describes the sequential incorporation of new sensors, starting with a known zero-strain notch frequency and maximum strain, and calculating

the notch frequency and resolution. In the second approach, we start with the full frequency spectrum and sensor count and then determine the maximum strain and resolution. This section focuses on the final mathematical *results*, with extended versions of the calculations and numerical design examples presented in the supplemental materials. Here we assume that the sensor nodes need to be completely spectrally isolated in their supported operational range. However, this is not a requirement of the notch encapsulation more generally: As mentioned briefly in III-C.2 and depicted in Fig. 4, sensor responses can overlap without adversely affecting the network response. The superimposed sensor responses simply alias each other. More advanced tracking approaches can be taken to disambiguate signal responses, which can allow more sensors to fit on the same network by allowing some overlap of the response. Our results provide a more conservative starting point and some theoretical grounding for a network design that does not require sophisticated algorithms to operate.

A. Preliminaries

In the sections that follow, it will be useful to have a few design terms specified. First, there is a particular mapping from a tensile strain to the resulting notch frequency. We define a model $f : \mathcal{S} \mapsto \mathcal{F}$ that maps the feasible range of strains $\mathcal{S} = [0, \varepsilon_1]$ onto the notch frequency bandwidth $\mathcal{F} = [f_1, f_0]$, where ε_1 is the maximum strain, f_1 is the frequency at the maximum strain ε_1, and f_0 is the zero-strain frequency at $\varepsilon = 0$. A negative relationship between strain and frequency is assumed (i.e., $f_1 < f_0$), consistent for models with positive gauge factors $G > 0$. The primary motivation to explicitly state $\mathcal{S}$ is to provide a constraint for parameter identification. If ε can grow unbounded, the lower bound on every sensor element is $f_1 = 0\,\text{Hz}$, which makes the design of a network impossible and is physically unrealizable. Furthermore, ε_1 is not simply a *physical constraint* but rather a *design consideration*: the maximum strain used in designing a network should be the maximum strain *expected* given the application plus some tolerance. Otherwise, the bandwidth required for each sensor may be excessive and limit the number of sensors that can be incorporated within a given bandwidth. The available sensing bandwidth is not unbounded either, but is dependent on our ability to generate an interrogating signal over the entire sensing bandwidth, sample at a rate high enough to capture the waveforms with low noise, and sample at a frequency high enough for the application.

The sensing resolution is controlled by two parameters: Δf_r, the frequency resolution; and $\Delta\varepsilon_r$, the strain resolution. The frequency resolution is bounded below by the reciprocal of the sampling period and above by the Nyquist frequency given the ADC sampling rate. It is assumed that the signal generator is capable of delivering spectral energy uniformly in the chirp bandwidth, which can be verified by computing the PSD of a chirp and confirming the uniform energy in the detection bandwidth. For practical frequencies (say, $1\,\text{kHz}$ to $100\,\text{kHz}$) this is easily achieved. The frequency resolution is then a tunable parameter of the PSD generation, which trades off resolution for noise. The strain resolution is more likely to be the designed parameter: what frequency resolution is required to give a particular strain resolution? In other cases, it might just be a fall-out of another design choice: given a bandwidth and sensor density, what is the best strain resolution? With that, we can start the network design.

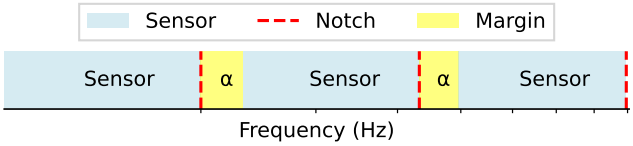

Fig. 5: Spectral placement of sequential filters. Shaded blue regions represent a sensor's full-strain frequency bandwidth. The zero-strain notch is indicated by a red, vertical dashed line. The gray shaded regions represent the margin α between sensors.

B. Building a network sequentially

Suppose that we want to add sensors sequentially in a network. Since models are added one by one, each filter is designed independently, and there is no need to assume homogeneity. For a given sensor, assume a particular model of the frequency response to strain, for example, the direct sensor connection to a Bainter notch filter as described in equation 6. Assume a known zero-strain starting frequency f_1 and a maximum strain ε_1. Note that in this case we are designing from the frequency at maximum strain, i.e., $f_1 = f(\varepsilon_1)$. Fig. 5 demonstrates why this is useful from the perspective of adding sensors sequentially: we always know the boundary condition of the previous sensor, i.e., the notch frequency; we know how close we want the max strain frequency f_1 to be, what we do not know is where the next zero-strain notch frequency is located.

We start by ignoring any margin between sensors (the α term in Fig. 5), so the zero-strain (notch) frequency of one sensor is the max-strain frequency of the next. For the direct connection model, there is nothing to tune except the gauge factor. We can determine the zero-strain notch frequency with a particular gauge factor by simply rearranging equation 6. The sensor bandwidth is completely determined by the gauge factor of the strain sensor used. Although this was determined for the simplest case, it is worth noting that, as long as the gauge factor is constant given a value of ε, that is, it has no dependence on frequency or any other factor that changes during operation, then we can generalize the relationship and relate f_1 and f_0 to any function Γ of ε only:

$$\begin{aligned} \Gamma(\varepsilon) &= \frac{f(\varepsilon) - f_0}{f_0} \\ f(\varepsilon) &= f_0\left(1 - \Gamma(\varepsilon)\right). \end{aligned} \tag{10}$$

Letting the constant $\Gamma_1 = \Gamma(\varepsilon_1)$, we have

$$f_1 = f_0(1 + \Gamma_1), \tag{11}$$

$$f_0 = f_1(1 + \Gamma_1)^{-1}. \tag{12}$$

With a known gauge factor, notch frequency, and frequency at maximum strain, we can derive a relationship between the strain resolution $\Delta\varepsilon_r$ and frequency resolution Δf_r. To achieve this frequency resolution we need to satisfy the following constraint:

$$\begin{aligned}\Delta f_r &\leq f(\varepsilon_1 - \Delta\varepsilon_r) - f(\varepsilon_1) \\ &= f_0(1 + \Gamma(\varepsilon_1 - \Delta\varepsilon_r)) - f_0(1 + \Gamma_1) \\ &= f_0(\Gamma(\varepsilon_1 - \Delta\varepsilon_r) - \Gamma_1).\end{aligned}$$

The resolutions depend heavily on the particular topology and the underlying model, so unfortunately the relationship will not reduce further. It is worth noting that the frequency resolution should be *higher* than the resolution used for the PSD generation to avoid quantization errors and ensure the desired strain resolution is achieved. The minimum required sampling period, independent of sampling frequency, is then

$$T_{\min} = \frac{1}{\Delta f_r}, \tag{13}$$

but choosing this sampling period exactly means that the periodogram estimate to achieve a resolution of Δf_r will be very noisy. This should be scaled up, perhaps ten times, to benefit from Welch's method.

Another consideration regarding the strain resolution is that it can be bounded by the frequency resolution. The frequency resolution is largely a hardware limitation, so typically the designer will like to know how fine the strain resolution can be given the hardware constraints. We can relate both terms to their respective bandwidths to compare them in terms of discrete, resolvable points. For strain, the bandwidth goes from zero to the maximum supported strain ε_1. Therefore, given a desired resolution $\Delta\varepsilon_r$, we expect the number of resolvable points to be at least

$$N_{\varepsilon,\text{desired}} = \left\lfloor \frac{\varepsilon_1}{\Delta\varepsilon_r} \right\rfloor. \tag{14}$$

The frequency bandwidth ranges from f_1 to f_0 resulting in a bandwidth of $f_0 - f_1 = -f_0\Gamma_1$. The number of resolvable frequency points in the sensor bandwidth is then

$$N_f = \left\lfloor \frac{f_0 - f_1}{\Delta f_r} \right\rfloor = \left\lfloor \frac{-f_0\Gamma_1}{\Delta f_r} \right\rfloor. \tag{15}$$

There can only be as many resolvable strain detections as there are for the frequency detection, so we can update our definition of (14) to

$$N_\varepsilon = \min\left\{N_{\varepsilon,\text{desired}}, N_f\right\}. \tag{16}$$

The finest strain resolution possible given the frequency resolution gives us a lower bound, namely

$$\Delta\varepsilon_r \geq \frac{\varepsilon_1}{N_f}. \tag{17}$$

This is useful to keep in mind to avoid trying to design a network with infeasible constraints.

In the direct case, the only variables that can be tuned are the gauge factor and strain resolution. In other configurations, we may also want to find reasonable values for one or more ratios k_i and one or more gauge factors G_i. In that case, it is helpful to consider an optimization problem using the constraints derived above, minimizing bandwidth and strain resolution while maximizing frequency resolution. Ideally, the sensor has a small bandwidth and fine strain resolution, but larger frequency resolution to reduce noise in the PSD computation. This can be accomplished using a sequential least squares program or more general nonlinear program using an interior point method.

C. Bounding the sensor limit for a given bandwidth

Suppose we have a given bandwidth and we would like to know how many sensors can be packed into that limited space. If we can assume that the model Γ is the same (i.e., all sensors have the same topology) and that the desired maximum strain is the same for each sensor, this can easily be derived. If the system is not homogeneous, the following approach can still be used to estimate the maximum density, but simplifying assumptions need to be made, for example choosing the *average* model and *average* strain. Otherwise, the sequential approach from section IV-B should be used.

Suppose that we want to place a sensor network in the bandwidth $[f_L, f_H]$ Hz, assuming a uniform maximum strain ε_1 for each sensor with underlying model $\Gamma(\varepsilon)$. We want to find N, the number of sensors that can be placed in this bandwidth. $\Gamma(\varepsilon_1) = \Gamma_1$, a constant. Starting from f_L, we can determine the frequency of the first notch, $f_1 = f_L(1+\Gamma_1)^{-1}$. In this section, f_n will indicate the n-th notch, a slight deviation from its previous use. Having established the first sensor's starting frequency f_1, we can move on to the second, which will operate from $f_2 = f_1(1 + \Gamma_1)^{-1}$ to $f_1 = f_L(1 + \Gamma_1)^{-1}$. The recursive relationship can now be seen and we can describe the full bandwidth in terms on N, noting that f_H is the notch frequency for the final sensor, i.e., $f_H = f_N$:

$$f_H = f_L(1 + \Gamma_1)^{-N}. \tag{18}$$

Then to determine N, we compute the logarithm of both sides of the equation and rearrange terms:

$$N = \left\lfloor \frac{\log(f_L/f_H)}{\log(1 + \Gamma_1)} \right\rfloor. \tag{19}$$

Notably absent from this determination is any sort of margin. If we can specify a margin in the form of a constant multiplied by the notch frequency f_{notch}, we can add it to the recursive form without too much trouble. One side of the $3\,\text{dB}$ bandwidth is such a margin that also makes some intuitive sense. Assuming that Q is constant,

$$\frac{1}{2}\text{BW}_{3\,\text{dB}} = \frac{f_{\text{notch}}}{2Q} = \alpha f_{\text{notch}}, \tag{20}$$

where $\alpha = 1/2Q$ is a constant and f_{notch} is the notch frequency. Note that the first sensor does not need a margin at the notch frequency, it can align exactly on the specified bandwidth. Also note only half the $3\,\text{dB}$ bandwidth was used, since only one side of the bandwidth should potentially

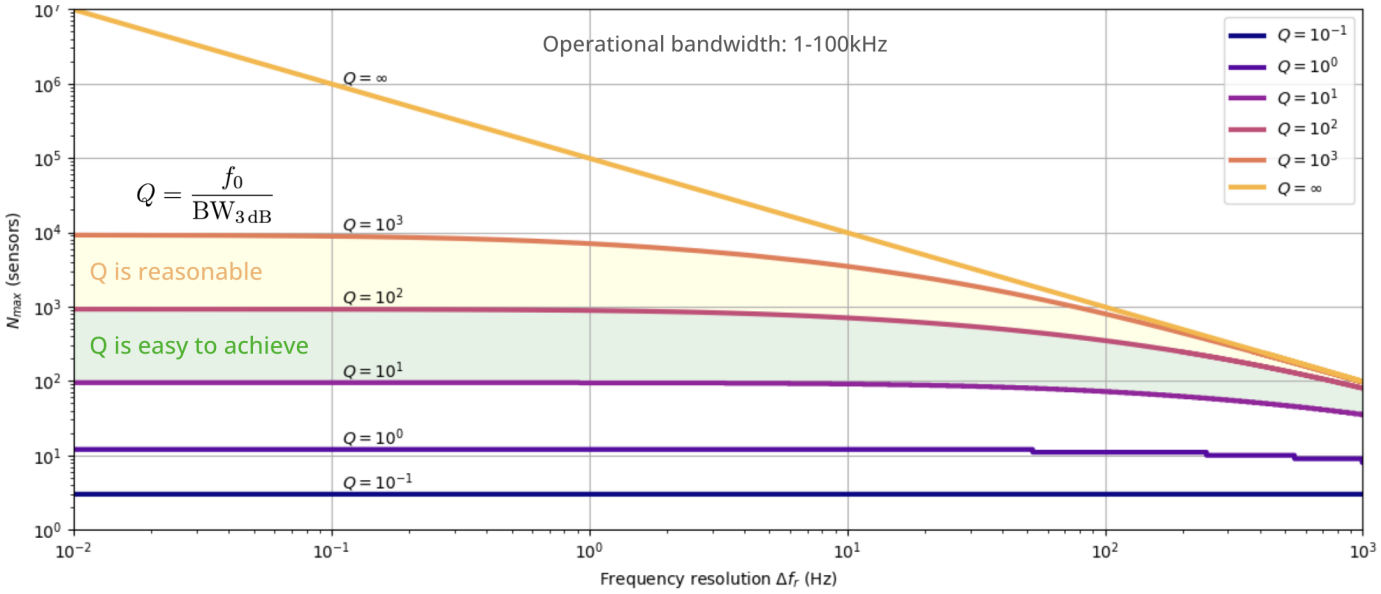

Fig. 6: Theoretical maximum sensor count given the frequency resolution Δf_r for a total bandwidth between 1 kHz to 100 kHz plotted for different values of Q. $Q = \infty$ is the limiting zero-margin (i.e., $\alpha = 0$) case. Otherwise, the margin is half the 3 dB bandwidth.

interfere with the adjacent sensor. Revisiting our recursive rules, we can describe the full bandwidth in terms of N:

$$f_H = f_L(1+\alpha)^{N-1}(1+\Gamma_1)^{-N}. \tag{21}$$

N is found again by computing the logarithm and rearranging terms:

$$N_\alpha = \left\lfloor \frac{\log(f_L/f_H) - \log(1+\alpha)}{\log(1+\Gamma_1) - \log(1+\alpha)} \right\rfloor \tag{22}$$

If there is no bandwidth, equation 22 reduces to 19 as expected. Alternatively, if we already knew how many sensors we wanted to place and either the lower or upper limit of the bandwidth, we can use equation 21 to determine the required bandwidth. As before, the frequency and strain resolution are completely determined by the particular topology and the lower frequency f_L.

We may be interested in the theoretical sensor limit in a given bandwidth. This is easy to define knowing only the bandwidth $[f_L, f_H]$ and the frequency resolution Δf_r. In the most extreme case, you only need one bit of resolution to qualify a sensor as having detected something. This limiting case may be useful if the device being designed only needs to detect that the strain exceeded some threshold, therefore only binary signal is required. Recalling the relations in equation 15, with no margin, the number of sensors that can fit in a bandwidth given only one resolvable point is just

$$N_{\max} = N_f = \left\lfloor \frac{f_H - f_L}{\Delta f_r} \right\rfloor. \tag{23}$$

Here we make the assumption that we can form some network that yields one resolvable frequency shift at the desired strain. No assumption of homogeneity is made. In fact, the sensor cell design constraints cannot be homogeneous or the sensor limit will be much lower, governed by equation 19 instead. More realistically, we will want to maintain some margin. Assuming a margin α again that scales with the notch frequency, we can see there is a term $f_L + \Delta f_r$ scaled by $(1+\alpha)^{N-1}$, along with a geometric series with $N-2$ terms, i.e.,

$$f_N = f_H = (f_L + \Delta f_r)(1+\alpha)^{N-1} + \sum_{k=0}^{N-2} \Delta f_r (1+\alpha)^k. \tag{24}$$

the geometric series can be rewritten in closed form, and we can take a logarithm and solve for N. Doing so yields

$$N_{\max,\alpha} = \left\lfloor 1 + \frac{\log\left(\frac{f_H + \Delta f_r/\alpha}{f_L + \Delta f_r(\alpha+1)/\alpha}\right)}{\log(1+\alpha)} \right\rfloor \tag{25}$$

for $\alpha > 0$. For a bandwidth of 1 kHz to 2 kHz, $Q = 25$, $\alpha = 1/Q$, and a frequency resolution of $\Delta f_r = 100$ Hz, this yields a maximum sensor count of 6. If the frequency resolution is set to 10 Hz instead, the sensor count goes up to 15. Increasing the notch Q-factor to 100 allows for 41 sensors. If there is no margin at all we would instead use equation 23 there would be room for 100 sensors. Using the original parameters but spanning instead from 1 kHz to 10 kHz, 32 sensors could be fit. Fig. 6 gives some intuitive insight to the upper limits. Limits on sensor count as a function of the frequency resolution are plotted for a handful of Q values. The quality factor determines the margin, which is the largest factor in this limiting case. These plots represent the upper bounds on sensor density under the very restrictive assumption of binary detection. When greater measurement fidelity is required, these numbers will decrease.

V. Conclusion

We have demonstrated that encapsulating resistive or capacitive sensors in notch filters is an effective method for creating distributed sensor networks, and showed embodiments in stretchable strain sensors. Encapsulation provides sensor isolation, facilitating network reconfiguration and device modularity. Fixed resistors and capacitors can be used to tune the sensor response and sensitivity. The simple interface allows for easy connection of many sensors on a single network using only a few wires for the interface. These factors make such a network amenable to different design requirements for such networks, whether on electronic skins or oddly shaped robots. To facilitate broader adoption, we additionally presented design principles for network design, emphasizing the tradoffs from both electrical and mechanical perspectives.

The framework we developed offers guidelines and first-principles theory to aid in designing such networks, but there are many unexplored areas that could provide further benefits in various applications. First, we used an oxidized liquid metal paste for the capacitive sensor electrodes. OGaIn has very high conductivity, so this works quite well in practice. However, if LMEE composites are used instead, the increased electrode resistance will affect the frequency response and may begin to diminish the observed capacitance at higher frequencies, as higher frequencies may not be able to penetrate the entire electrode as observed in previous works [19], [21], [22]. Next, while resistive strain sensors are covered in the theory developed and treated equivalently to capacitive sensors, the models were derived under the assumption of linear sensor response. This is typical of capacitive sensors and a major benefit to using them, but resistive sensors can show considerably greater nonlinearity, especially at high strains. In this work, we did not thoroughly evaluate the effect of nonlinear response in either the sensors or nonideal component operation. These could be of great importance for applications operating in more extreme conditions or with more variable components. Finally, we did not examine the effects of hysteresis, which can arise from differences in electromechanical coupling during elastic stretch and relaxation. Capacitive sensors typically exhibit low hysteresis, so this was largely unobserved in our experiments, but hysteresis can be substantial in resistive sensors. By further characterizing these areas and building upon advances in stretchable electronics, we envision this approach to multimodal sensing to allow higher sensor density on the surface of soft robots and wearables.

References

[1] J. Yin, T. Hellebrekers, and C. Majidi, "Closing the loop with liquid-metal sensing skin for autonomous soft robot gripping," in *2020 3rd IEEE International Conference on Soft Robotics (RoboSoft)*, IEEE, 2020, pp. 661–667.

[2] W. Dou, G. Zhong, J. Cao, Z. Shi, B. Peng, and L. Jiang, "Soft robotic manipulators: Designs, actuation, stiffness tuning, and sensing," *Advanced Materials Technologies*, vol. 6, no. 9, p. 2 100 018, 2021.

[3] R. L. Truby, C. Della Santina, and D. Rus, "Distributed proprioception of 3d configuration in soft, sensorized robots via deep learning," *IEEE Robotics and Automation Letters*, vol. 5, no. 2, pp. 3299–3306, 2020.

[4] D. S. Shah, S. J. Woodman, T. L. Buckner, E. J. Yang, and R. K. Kramer-Bottiglio, "Robotic skins with integrated actuation, sensing, and variable stiffness," *IEEE Robotics and Automation Letters*, 2023.

[5] C. Hegde, J. Su, J. M. R. Tan, K. He, X. Chen, and S. Magdassi, "Sensing in soft robotics," *ACS nano*, vol. 17, no. 16, pp. 15 277–15 307, 2023.

[6] B. Shih, D. Shah, J. Li, *et al.*, "Electronic skins and machine learning for intelligent soft robots," *Science Robotics*, vol. 5, no. 41, eaaz9239, 2020.

[7] J. Yin, R. Hinchet, H. Shea, and C. Majidi, "Wearable soft technologies for haptic sensing and feedback," *Advanced Functional Materials*, vol. 31, no. 39, p. 2 007 428, 2021.

[8] P. Roberts, M. Zadan, and C. Majidi, "Soft tactile sensing skins for robotics," *Current Robotics Reports*, vol. 2, pp. 343–354, 2021.

[9] D. Shah, S. J. Woodman, L. Sanchez-Botero, S. Liu, and R. Kramer-Bottiglio, "Stretchable shape-sensing sheets," *Advanced Intelligent Systems*, vol. 5, no. 12, p. 2 300 343, 2023.

[10] L. A. Ngiejungbwen, H. Hamdaoui, and M.-Y. Chen, "Polymer optical fiber and fiber bragg grating sensors for biomedical engineering applications: A comprehensive review," *Optics & Laser Technology*, vol. 170, p. 110 187, 2024.

[11] M. Park, T. Park, and Y.-L. Park, "Parametric analysis of multi-material soft sensor structures for enhanced strain sensitivity," *Extreme Mechanics Letters*, vol. 60, p. 101 983, 2023.

[12] C. Majidi, K. Alizadeh, Y. Ohm, A. Silva, and M. Tavakoli, "Liquid metal polymer composites: From printed stretchable circuits to soft actuators," *Flexible and Printed Electronics*, vol. 7, no. 1, p. 013 002, 2022.

[13] H. Nesser and G. Lubineau, "Strain sensing by electrical capacitive variation: From stretchable materials to electronic interfaces," *Advanced Electronic Materials*, vol. 7, no. 10, p. 2 100 190, 2021.

[14] S. Wu, S. Peng, Y. Yu, and C.-H. Wang, "Strategies for designing stretchable strain sensors and conductors," *Advanced Materials Technologies*, vol. 5, no. 2, p. 1 900 908, 2020.

[15] H. Souri, H. Banerjee, A. Jusufi, *et al.*, "Wearable and stretchable strain sensors: Materials, sensing mechanisms, and applications," *Advanced Intelligent Systems*, vol. 2, no. 8, p. 2 000 039, 2020.

[16] R. Bhirangi, T. Hellebrekers, C. Majidi, and A. Gupta, "Reskin: Versatile, replaceable, lasting tactile skins," in *5th Annual Conference on Robot Learning*, 2021.

[17] B. C.-K. Tee, A. Chortos, A. Berndt, *et al.*, "A skin-inspired organic digital mechanoreceptor," *Science*, vol. 350, no. 6258, pp. 313–316, 2015.

[18] M. Kaltenbrunner, T. Sekitani, J. Reeder, *et al.*, "An ultra-lightweight design for imperceptible plastic electronics," *Nature*, vol. 499, no. 7459, pp. 458–463, 2013.

[19] E. L. White, M. C. Yuen, and R. K. Kramer, "Distributed sensing in capacitive conductive composites," in *2017 IEEE SENSORS*, IEEE, 2017, pp. 1–3.

[20] A. Tairych and I. A. Anderson, "Distributed sensing: Multiple capacitive stretch sensors on a single channel," in *Electroactive Polymer Actuators and Devices (EAPAD) 2017*, SPIE, vol. 10163, 2017, p. 1 016 306.

[21] A. Tairych and I. A. Anderson, "A numerical method for measuring capacitive soft sensors through one channel," *Smart Materials and Structures*, vol. 27, no. 3, p. 035 016, 2018.

[22] H. A. Sonar, M. C. Yuen, R. Kramer-Bottiglio, and J. Paik, "An any-resolution pressure localization scheme using a soft capacitive sensor skin," in *2018 IEEE International Conference on Soft Robotics (RoboSoft)*, IEEE, 2018, pp. 170–175.

[23] H. Bai, S. Li, J. Barreiros, Y. Tu, C. R. Pollock, and R. F. Shepherd, "Stretchable distributed fiber-optic sensors," *Science*, vol. 370, no. 6518, pp. 848–852, 2020.

[24] T. Hellebrekers, O. Kroemer, and C. Majidi, "Soft magnetic skin for continuous deformation sensing," *Advanced Intelligent Systems*, vol. 1, no. 4, p. 1 900 025, 2019.

[25] D. Kim and Y.-L. Park, "Contact localization and force estimation of soft tactile sensors using artificial intelligence," in *2018 IEEE/RSJ International Conference on Intelligent Robots and Systems (IROS)*, IEEE, 2018, pp. 7480–7485.

[26] J. Å. Stakvik, M. R. P. Ragazzon, A. A. Eielsen, and J. T. Gravdahl, "On implementation of the preisach model identification and inversion for hysteresis compensation," 2015.

[27] S. Funabashi, T. Isobe, F. Hongyi, *et al.*, "Multi-fingered in-hand manipulation with various object properties using graph convolutional networks and distributed tactile sensors," *IEEE Robotics and Automation Letters*, vol. 7, no. 2, pp. 2102–2109, 2022.

[28] J. Kim, S. Kim, and Y.-L. Park, "Single-input single-output multi-touch soft sensor systems using band-pass filters," *npj Flexible Electronics*, vol. 6, no. 1, p. 65, 2022.

[29] J. Kim, J. Kim, and Y.-L. Park, "Multi-modal modular textile sensor for physical human–robot interaction using band-stop filters," *Advanced Functional Materials*, vol. 34, no. 7, p. 2 308 571, 2024.

[30] A. B. Williams, "Band-reject filters," en, in (Analog Filter and Circuit Design Handbook), 1st Edition, Analog Filter and Circuit Design Handbook. New York: McGraw-Hill Education, 2014, ISBN: 9780071816717. [Online]. Available: https://www.accessengineeringlibrary.com/content/book/9780071816717/chapter/chapter6.

[31] J. R. Bainter, "Active filter has stable notch, and response can be regulated," *Electronics*, vol. 48, pp. 115–117, 1975.

[32] P. Roberts, D. D. Damian, W. Shan, T. Lu, and C. Majidi, "Soft-matter capacitive sensor for measuring shear and pressure deformation," in *2013 IEEE International Conference on Robotics and Automation*, IEEE, 2013, pp. 3529–3534.

[33] M. D. Bartlett, E. J. Markvicka, and C. Majidi, "Rapid fabrication of soft, multilayered electronics for wearable biomonitoring," *Advanced Functional Materials*, vol. 26, no. 46, pp. 8496–8504, 2016.

[34] M. Reis Carneiro, C. Majidi, and M. Tavakoli, "Gallium-based liquid–solid biphasic conductors for soft electronics," *Advanced Functional Materials*, vol. 33, no. 41, p. 2 306 453, 2023.

[35] P. Welch, "The use of fast fourier transform for the estimation of power spectra: A method based on time averaging over short, modified periodograms," *IEEE Transactions on audio and electroacoustics*, vol. 15, no. 2, pp. 70–73, 1967.

[36] A. Savitzky and M. J. Golay, "Smoothing and differentiation of data by simplified least squares procedures.," *Analytical chemistry*, vol. 36, no. 8, pp. 1627–1639, 1964.

[37] J. J. Moré, "The levenberg-marquardt algorithm: Implementation and theory," in *Numerical analysis: proceedings of the biennial Conference held at Dundee, June 28–July 1, 1977*, Springer, 2006, pp. 105–116.